ISSN 0915-633X

INTERNATIONAL ATOMIC ENERGY AGENCY

FIFTEENTH INTERNATIONAL CONFERENCE ON PLASMA PHYSICS AND CONTROLLED NUCLEAR FUSION RESEARCH

Seville, Spain, 26 September – 1 October 1994

IAEA-CN-60/D-P-I-11

NATIONAL INSTITUTE FOR FUSION SCIENCE

Dynamical Model of Pressure-Gradient-Driven Turbulence and Shear Flow Generation in L-H Transition

H. Sugama and W. Horton

(Received - Aug. 23, 1994)

NIFS-300 Aug. 1994

RESEARCH REPORT
NIFS Series

NAGOYA, JAPAN

INTERNATIONAL ATOMIC ENERGY AGENCY

FIFTEENTH INTERNATIONAL CONFERENCE ON PLASMA PHYSICS AND CONTROLLED NUCLEAR FUSION RESEARCH

Seville, Spain, 26 September – 1 October 1994

IAEA-CN-60/D-P-I-11

Dynamical Model of Pressure-Gradient-Driven Turbulence and Shear Flow Generation in L-H Transition

H. SUGAMA

National Institute for Fusion Science, Chikusaku, Nagoya 464-01, Japan

W. HORTON

Institute for Fusion Studies, The University of Texas at Austin, Austin, Texas 78712, USA

KEYWORDS: pressure-gradient-driven turbulence, shear flow, L-H transition, Reynolds stress,

Dynamical Model of Pressure-Gradient-Driven Turbulence and Shear Flow Generation in L-H Transition

ABSTRACT

We present a dynamical model for the L-H transition consisting of three ordinary differential equations. This model describes temporal evolutions of three charcterisistic variables, i.e., the free energy contained in the pressure gradient, the turbulent kinetic energy and the shear flow energy in the resistive pressure-gradient-driven turbulence. The model equations have stationary solutions corresponding to the L and H-modes and their stabilities depend on the energy input to the peripheral region. Changing the energy input parameter yields the L to H and H to L transitions. We also find the parameter region in which the H-mode stationary solution becomes unstable and bifurcate to the limit cycle which shows periodic oscillations like ELM. It depends on the viscosity for the shear flow which the type of the L-H transition is, a first-order or second-order transition.

1. INTRODUCTION

Various theoretical models have been proposed in recent years in order to explain the mechanism of the L-H transitions observed in many tokamaks and in some stellarators. The key points, which such models attempt to describe, are how the radial electric field or the poloidal shear flow suppresses the turbulence and anomalous transport and how the electric field or the shear flow is produced. Concerning the mechanism of the shear flow generation, some models are based on the particle orbit loss processes [1,2] and others are based on the turbulent processes or Reynolds stress [3–8]. In the latter, the divergence of the Reynolds stress or the nonlinear convective term in the momentum equation drives the plasma flow. In the L-H transition model presented in this work, the Reynolds stress is considered to be the cause of the shear flow generation. Diamond et al. [5,6] presented a simple L-H transition model consisting of two ordinary differential equations which describes the temporal behavior of the turbulent fluctuation and the shear flow although the pressure gradient is fixed as a control parameter. In actual experiments, the pressure gradient also changes at the L-H transition according to the change in the transport. Therefore, our model extends their model by including the pressure gradient as a basic variable as well as the fluctuation and the flow. Then the physically novel features, not contained in theirs, appear in ours as is described later.

2. MODEL EQUATIONS AND STABILITY OF STATIONARY SOLUTIONS

Basic variables for our dynamical model of L-H transtion are the turbulent kinetic energy K, the background shear flow kinetic energy F, and the potential energy related to the pressure profile U, which are defined by

$$K \equiv \frac{1}{\delta}\int_{-\delta}^{0} dx \frac{1}{2}\langle \tilde{v}^2 \rangle, \quad F \equiv \frac{1}{\delta}\int_{-\delta}^{0} dx \frac{1}{2} v_0^2, \quad U \equiv \frac{1}{\delta}\int_{-\delta}^{0} dx \frac{(-x)}{L_c}\frac{P_0}{n_0 m_i} \tag{1}$$

respectively, where we define the peripheral region by $-\delta \leq x \leq 0$. Here, the angle bracket $\langle\cdot\rangle$ denotes the average over the (y, z)-plane (or the magnetic surface). The velocity and the pressure are divided into the x-dependent average parts and the fluctuating parts as $\boldsymbol{v} = \boldsymbol{v}_0(x) + \tilde{\boldsymbol{v}}$ and $p = p_0(x) + \tilde{p}$, respectively. The average mass density is denoted by $n_0 m_i$. The unfavorable magnetic curvature is represented by $1/L_c$ and is assumed to be constant. From the reduced resistive MHD equations [7–9] in the electrostatic approximation, we obtain the following energy balance equations

$$\begin{aligned} dU/dt &= P_U - P_K &(2)\\ dK/dt &= P_K - P_F - \epsilon_K &(3)\\ dF/dt &= P_F - \epsilon_F &(4) \end{aligned}$$

where the production and dissipation terms in the right-hand sides are given by

$$P_U \equiv \frac{\langle \tilde{p}\tilde{v}_x \rangle|_{x=-\delta}}{L_C n_0 m_i}, \quad P_K \equiv \frac{1}{\delta}\int_{-\delta}^{0} dx \frac{\langle \tilde{p}\tilde{v}_x \rangle}{L_C n_0 m_i}, \quad P_F \equiv \frac{1}{\delta}\int_{-\delta}^{0} dx \langle \tilde{v}_x \tilde{v}_y \rangle \frac{dv_0}{dx}$$

$$\epsilon_K \equiv \frac{1}{\delta}\int_{-\delta}^{0} dx \left\{ \mu \left\langle \left(\frac{\partial \tilde{v}_i}{\partial x_j} \right)^2 \right\rangle + \frac{\eta}{n_0 m_i} \langle \tilde{J}_{\parallel}^2 \rangle \right\}, \quad \epsilon_F \equiv \frac{1}{\delta}\int_{-\delta}^{0} dx \mu \left(\frac{dv_0}{dx} \right)^2 .$$

Here μ denotes the (kinematic) viscosity, η the resistivity and $\tilde{J}_{\parallel} = \eta^{-1}\nabla_{\parallel}\phi$ the parallel current. The electrostatic potential ϕ gives the velocity as $\boldsymbol{v} = -(c/B_0)\nabla\phi \times \hat{z}$ in the reduced MHD model. In the temporal evolution equation for U, we have neglected the collsional dissipation term by assuming that the turbulent thermal transport is much larger than the collisional one. The potential energy production P_U is given by the energy input to the peripheral region through the inner boundary at $x = -\delta$, the turbulent energy production P_K is expressed in terms of the pressure transport multiplied by the unfavorable curvature, which is originally from the potential energy, and the background flow production is represented by the product of the Reynolds stress and the flow shear, which comes from the turbulent kinetic energy. As for the dissipation terms. ϵ_K stands for the viscous and Joule dissipations of the fluctuation, and ϵ_F the viscous dissipation of the average flow.

Estimating the time scale τ_c in the g or ballooning mode turbulence as $\tau_c \sim [t] \equiv (L_c n_0 m_i/|dP_0/dx|)^{1/2}$ and approximating $U \sim \delta^2 |dP_0/dx| /(L_c n_0 m_i)$ yield $\tau_c \sim \delta U^{-1/2}$. Giving the anomalous pressure diffusivity as $D \sim \tau_c K$. we have $P_K \sim D|dP_0/dx|/(L_c n_0 m_i) \sim \tau_c^{-1} K \sim \delta^{-1} U^{1/2} K$. From similar approximations for the Reynolds stress $\langle \tilde{v}_x \tilde{v}_y \rangle \sim \tau_c K(dv_0/dx)$ and the shear flow energy $F \sim \delta^2 (dv_0/dx)^2$, we obtain $P_F \sim \tau_c K(dv_0/dx)^2 \sim \delta^{-1} U^{-1/2} FK$. Assuming that the Joule dissipation is dominant in ϵ_K, the turbulent energy dissipation can be written as $\epsilon_K \sim D_L^{-1} K^2$ where $D_L = D_L(U)$ is the L-mode anomalous diffusivity [10] and a function of U through its dependence on the background temperature. This form of the turbulent energy dissipation $\epsilon_K \propto K^2$ is the same as in the Diamond's model [5,6]. Finally the background flow energy dissipation is written as $\epsilon_F \sim \mu \delta^{-2} F$ where the ion collisional viscosity $\mu = \mu(U)$ is also given as a function of U. Thus a closed set of the equations for U, K and F are obtained as follows

$$
\begin{aligned}
dU/dt &= P_U - C_K \delta^{-1} U^{1/2} K && (5)\\
dK/dt &= C_K \delta^{-1} U^{1/2} K - C_F \delta^{-1} U^{-1/2} FK - C'_K D_L^{-1} K^2 && (6)\\
dF/dt &= C_F \delta^{-1} U^{-1/2} FK - C'_F \delta^{-2} \mu F && (7)
\end{aligned}
$$

where the potential energy input $P_U (> 0)$ is regarded as an external or control parameter and C's are nondimensional numerical constants.

Introducing the following normalized variables, functions and parameters

$$
\begin{aligned}
&u = U/U_{c1}, \quad k = K/U_{c1}, \quad f = F/U_{c1}, \quad \tau = C_K \delta^{-1} U_{c1}^{1/2} t \\
&d(u) = C_K C_K'^{-1} \delta^{-1} U_{c1}^{-1/2} D_L(U), \quad m(u) = C_F^{-1} C'_F \delta^{-1} U_{c1}^{-1/2} \mu(U) \qquad (8)\\
&q = C_K^{-1} \delta U_{c1}^{-2/3} P_U, \quad c = C_F/C_K
\end{aligned}
$$

Eqs.(5)–(7) are rewritten as

$$
\begin{aligned}
du/d\tau &= q - u^{1/2} k && (9)\\
dk/d\tau &= u^{1/2} k - c u^{-1/2} f k - d^{-1}(u) k^2 && (10)\\
df/d\tau &= c u^{-1/2} f k - c m(u) f. && (11)
\end{aligned}
$$

Stationary solutions corresponding to the L and H mode stationary points are give by (u_L, k_L, f_L) and (u_H, k_H, f_H) respectively, where $k_L = u_L^{1/2} d(u_L)$, $f_L = 0$, $k_H = u_H^{1/2} m(u_H)$

and $f_H = c^{-1}u_H d^{-1}(u_H)(d(u_H) - m(u_H))$. Here u_L and u_H are functions of the control parameter q defined by $u_L d(u_L) = u_H m(u_H) = q$. The condition for the existence of the H-mode stationary solution is written as $d(u_H) > m(u_H)$. The critical value q_{c1} is give by solving $u_{c1}d(u_{c1}) = u_{c1}m(u_{c1}) = q_{c1}$. Here we define the normalization unit U_{c1} such that $u_{c1} = 1$. We consider the two cases where $ud(u)$ and $um(u)$ are functions of u as shown in Figs.1(a) and (b). In the case of Fig.1(b), the condition $d(u_H) > m(u_H)$ is equivalent to $q > q_{c1}$. In the case of Fig.1(a), the H-mode solution exists for $q > q_{c2}$ where q_{c2} is the minimum value of $um(u)$ at $u = u_{c2}(> u_{c1} \equiv 1)$. In this case, for $q_{c2} < q < q_{c1}$, the equation $um(u) = q$ has two solutions u_{H-} and $u_{H+}(> u_{H-})$ where u_{H-} is unstable and u_{H+} corresponds to the real H-mode.

Next, we examine linear stabilities of the L and H-mode stationary solutions. The eigenvalues of the matrix obtained by the linearizing the model equations around the L-mode solution are given by $\lambda_{L1} \equiv c(d_L - m_L)$, λ_{L+} and λ_{L-} where λ_{L+} and λ_{L-} are the solutions of the quadratic equations

$$\lambda^2 + \left(\frac{1}{2}d_L + u_L^{1/2}\right)\lambda + u_L^{1/2}(u_L d_L)' = 0. \tag{12}$$

Here $d_L \equiv d(u_L)$, $m_L \equiv m(u_L)$, $d'_L \equiv d'(u_L)$ and $'$ denotes the derivative with respect to u. We find that $\mathrm{Re}\lambda_{L+} < 0$ and $\mathrm{Re}\lambda_{L-} < 0$ since $(ud)' > 0$ is assumed as seen in Figs.1(a) and (b). The eigenvectors corresponding to λ_{L+} and λ_{L-} are both tangential to the (u, k)-plane defined by $f = 0$ and the L-mode solution $(u_L, k_L, 0)$ is a sink for the orbits on this plane. The L-mode solution is unstable if and only if $d_L > m_L$ which is equivalent to the condition $q > q_{c1}$.

The eigenvalues of the matrix obtained by the linearizing the model equations around the L-mode solution are given by the solutions of

$$\lambda^3 + A\lambda^2 + B\lambda + C = 0 \tag{13}$$

where $A = m_H\left(1/2 + u_H^{1/2}/d_H\right)$, $B = u_H^{1/2}m_H((1+c)(1 - m_H/d_H) + m_H(u_H d_H)'/d_H^2)$, $C = cu_H^{1/2}m_H(u_H m_H)'(1 - m_H/d_H)$, $d_H \equiv d(u_H)$, $m_H \equiv m(u_H)$ and $m'_H \equiv m'(u_H)$. Here we consider the case in which the condition for the existence of the H-mode solution $d_H > m_H$ is satisfied. It is found that both A and B are positive. In the case of $u_H = u_{H-}$ in Fig.1(a) where $q_{c2} < q < q_{c1}$, we obtain $C < 0$ since $(um)' < 0$ for $u_{c1} < u < u_{c2}$. Then the stationary point (u_{H-}, k_{H-}, f_{H-}) is unstable since Eq.(13) has one real and positive solution for $C < 0$. For the H-mode stationary point in Fig.1(b) and for that at $u > u_{c2}$ in

Fig.1(a), we have $C > 0$ and therefore at least one real and negative solution of Eq.(13). In these cases where $C > 0$, other two solutions of Eq.(13) are both real and negative or a pair of complex conjugate values since both A and B are positive. Thus the marginal stability of the H-mode solution except for (u_{H-}, k_{H-}, f_{H-}) occurs when $C = AB$ which implies that Eq.(13) has a pair of pure imaginary solutions. Then these H-mode solutions become unstable when $C > AB$ which is rewritten as

$$\frac{(u_H m_H)'}{m_H} > \left(1 + c^{-1} + c^{-1}\frac{m_H/d_H}{1 - m_H/d_H}\frac{(u_H d_H)'}{d_H}\right)\left(\frac{1}{2} + \frac{u_H^{1/2}}{d_H}\right). \tag{14}$$

This criterion for the instability of the H-mode depends on the values of q (through $u_H = u_H(q)$), c as well as the functional forms of $d(u)$ and $m(u)$. There appears a Hopf-bifurcation from the stable H-mode solution to the limit cycle around the unstable H-mode solution just when (14) is satisfied.

4. NUMERICAL MODELING AND DISCUSSION

Here numerical solutions of Eqs.(9)–(11) are given for two cases of the functions $d(u)$ and $m(u)$ based on neoclassical and turbulent viscosities. The dimensional analysis [11] gives the anomalous diffusivity in the resistive g and ballooning mode turbulence proportional to the pressure gradient, and we use $d(u) = u$ in all the numerical calculations reported here. The turbulent viscosity resulting from the small scale part of the turbulent inertia term is dominant for larger pressure gradients and given as $\sim c_\mu u$ where the positive constant c_μ is small since we consider that the low wavenumber part of the turbulent inertia term or the Reynolds stress generates shear flow against the viscous damping. For smaller pressure gradients, the neoclassical viscosity [12] given by $\mu_{nc} = Rqv_{Ti}\nu_{*i}/[(1+\nu_{*i})(1+\epsilon^{3/2}\nu_{*i})]$ with $\nu_{*i} = Rq\nu_i/v_{Ti}\epsilon^{3/2}$ is dominant for the damping of the mean shear flow. Here we model the teperature dependence of the viscosity by taking u proportional to T_i and introduce $m(u) \approx u^{-3/2}$ for small u in Case I as in the banana regime ($\nu_{*i} < 1$) and $m(u) \approx u^{-1}$ for low u in Case II as in the transitional regime ($\nu_{*i} \sim 1$). Thus, for the numerical studies we take $m(u) = u^{-3/2}(0.95 + 0.05u^{5/2})$ for Case I and $m(u) = u^{-1}(0.97 + 0.03u^2)$ for Case II. Case I and Case II correspond to the cases in Figs. 1(a) and (b), respectively. We put $c = 5$ for which we can satisfy the H mode instability criterion (14) for some values of q.

For Case I, we have $u_{c1} = 1$, $q_{c1} = 1$, $u_{c1}^* = 3.01$, $u_{c2} = 1.86$, $u_{c2}^* = 0.93$, $q_{c2} = 0.87$, $u_{c3} = 4.40$ and $q_{c3} = 1.42$, which are shown in Fig. 1(a). Here (q_{c3}, u_{c3}) denotes the critical point for the bifurcation of the H mode into the limit cycle associated with ELM state.

The solid and dashed curves in Fig. 1 correspond to the stable and unstable stationary solutions, respectively. For $q < q_{c2}$, there exists only one stationary solution, i.e., the stable L mode solution. For $q_{c2} < q < q_{c1}$, the L mode stationary solution remains stable while there appears one stable H mode solution and another unstable stationary solution. For $q_{c1} < q < q_{c3}$, the L mode stationary solution is unstable and the stable H mode solution appears. For $q > q_{c3}$, the L mode remains unstable and the H mode also becomes unstable. There appears a limit cycle around this unstable H mode solution. Thus we obtain the Hopf-bifurcation at $q = q_{c3} = 1.42$. Let us regard a value of u for the stable stationary solution as an 'order parameter' in our system and consider it as a function $u = u(q)$ of the control parameter q. Due to the parameter region $q_{c2} < q < q_{c1}$ where the two stable stationary solutions exist, we obtain the hysteresis curve of the order paramater $u = u(q)$ as shown by arrows in Fig. 1(a). At the critical points $q = q_{c1}$ and $q = q_{c2}$ of the L to H and H to L transitions, the order parameter u changes discontinuously with respect to q as $u_{c1} \to u^*_{c1}$ and $u_{c2} \to u^*_{c2}$. Thus the L-H transition is like a first-order phase transition for Case I where $\nu_{*i} < 1$ is required. In Fig. 2, we find the results where the control parameter is temporally varied, which corresponds to ramping up and down additional plasma heating power. Figure 2(a) shows the control parameter $q = q(\tau)$ as a function of time. The temporal dependence of (u, k, f) are shown in Figs. 2(b). The hysteresis nature can be clearly seen in that the L to H transition occurs when $q > q_{c1} = 1$ while the H to L transition occurs when $q < q_{c2} = 0.87$. We can also see that, while $q > q_{c3} = 1.42$, the ELM-like instability grows approaching to the periodic oscillation represented by the limit cycle.

For Case II, we have $u_{c1} = 1$, $q_{c1} = 1$, $u_{c3} = 6.28$ and $q_{c3} = 2.15$, which are shown in Fig. 1(b). For $q < q_{c1}$, there exists only one stationary solution, i.e., the stable L mode solution similar to that for $q < q_{c2}$ in Case I. For $q_{c1} < q < q_{c3}$ and $q > q_{c3}$, the stability of the L and H stationary solutions is the same as in the corresponding parameter regions for Case I. The Hopf-bifurcation is again found at $q = q_{c3} = 2.15$. At the critical point $q = q_{c1}$, the order parameter u as a function of the control parameter q is continuous while the its first derivative du/dq is not. No hysteresis is obtained. Thus the L-H transition in Case II is like a second-order phase transition. Finite change in q is required for finite change in u. In Fig. 3, the results where the control parameter is temporally varied are shown in the same way as in Fig. 2. Even though this case corresponds to the second-order transition, we find clear L to H and H to L transitions since certain time lag required to reach the bifurcated stable solution causes the finite difference in q and accordingly sudden changes in (u, k, f). The ELM-like oscillations are also seen for $q > q_{c3} = 2.15$.

REFERENCES

[1] ITOH, S.-I., ITOH. K., Phys. Rev. Lett. **60** (1988) 2276.

[2] SHAING, K. C., CRUME, JR. E. C., HOULBERG, W. A., Phys. Fluids B **2** (1990) 1492.

[3] DIAMOND, P. H., KIM, Y. -B., Phys. Fluids B **3** (1991) 1626.

[4] DRAKE, J. F., FINN, J. M., GUZDAR , P., SHAPIRO, V., SHEVCHENKO, V., WAELBROECK, F., HASSAM, A. B., LIU, C. S., SAGDEEF. R., Phys. Fluids B **4** (1992) 488.

[5] DIAMOND, P. H., SHAPIRO. V., SHEVCHENKO, V., KIM, Y. -B., ROSENBLUTH, M. N., CARRERAS, B. A., SIDIKMAN, K., LYNCH, V. E., GARCIA, L., TERRY, P. W., SAGDEEF, R. Z., in Plasma Physics and Controlled Nuclear Fusion Research, 1992, Proceedings of the 14th International Conference, Würzburg, Vol.2 (IAEA, Vienna, 1993) 97.

[6] DIAMOND, P. H., LIANG, Y. -M., CARRERAS, B. A., TERRY, P. W., Phys. Rev. Lett. **72** (1994) 2565.

[7] SUGAMA H., HORTON, W., Phys. Plasmas **1** (1994) 345.

[8] SUGAMA H., HORTON, W., Phys. Plasmas **1** (1994) 2220.

[9] STRAUSS, H. R., Plasma Phys. **22** (1980) 733.

[10] SUGAMA, H., OKAMOTO, M., WAKATANI, M., in Plasma Physics and Controlled Nuclear Fusion Research, 1992, Proceedings of the 14th International Conference, Würzburg, Vol.2 (IAEA, Vienna, 1993) 353.

[11] CONNOR, J. W., Plasma Phys. Controll. Fusion **30** (1988) 619.

[12] HIRSHMAN, S. P., Phys. Fluids **21** (1978) 224.

FIGURE CAPTIONS

FIG.1. Stationary solutions in the (u, q)-plane. (a) Case I ($\nu_{*1} < 1$); (b) Case II ($\nu_{*1} \sim 1$). The solid and dashed curves correspond to the stable and unstable solutions, respectively.

FIG.2. Numerical solutions for Case I where the energy input is temporally varied. (a) The energy input parameter q as a function of time. (b) The temporal dependence of (u, k, f).

FIG.3. Numerical solutions for Case II where the energy input is temporally varied. (a) The energy input parameter q as a function of time. (b) The temporal dependence of (u, k, f).

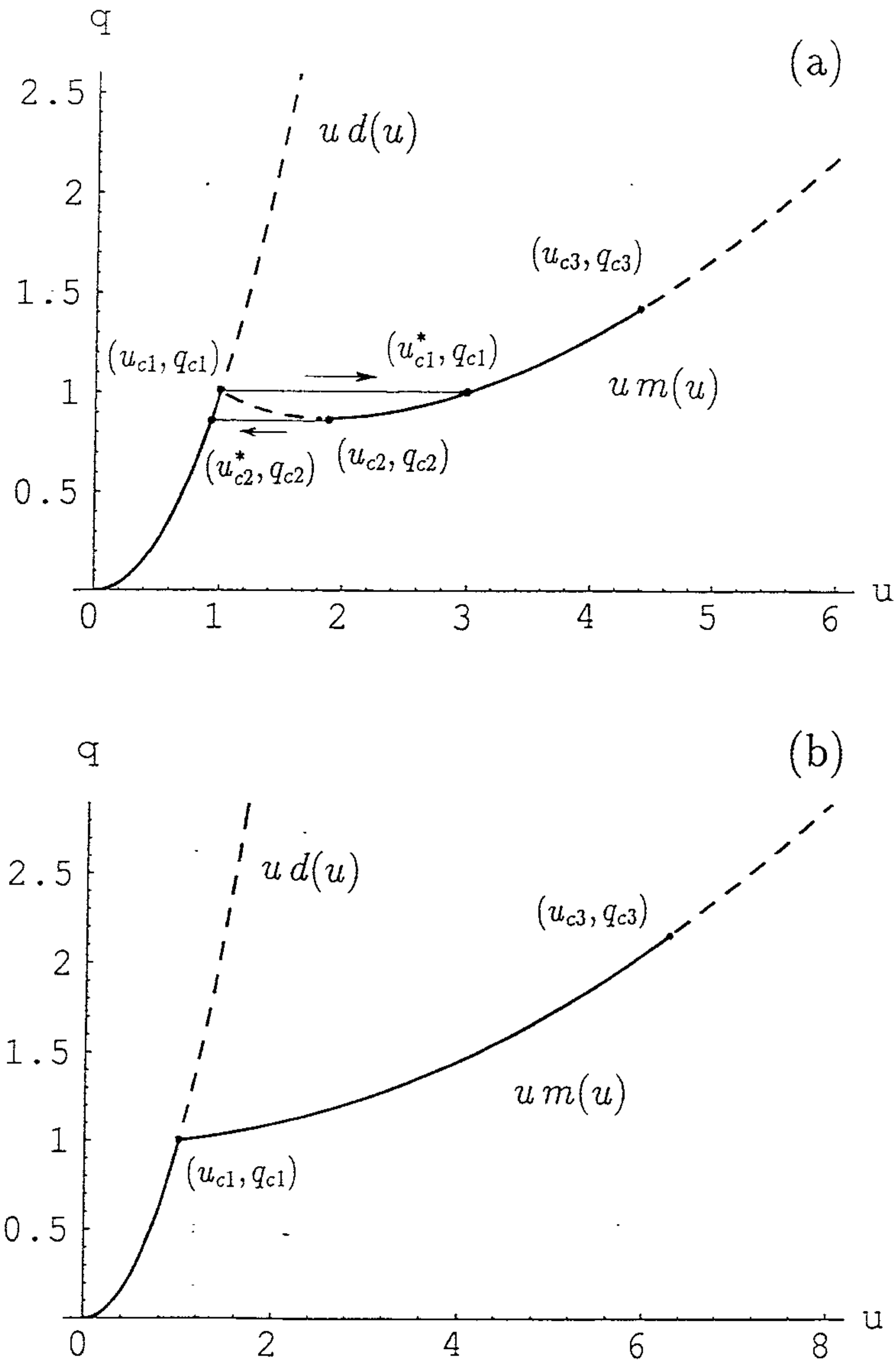

FIG.1. Stationary solutions in the (u, q)-plane. (a) Case I ($\nu_{*i} < 1$). (b) Case II ($\nu_{*i} \sim 1$). The solid and dashed curves correspond to the stable and unstable solutions, respectively.

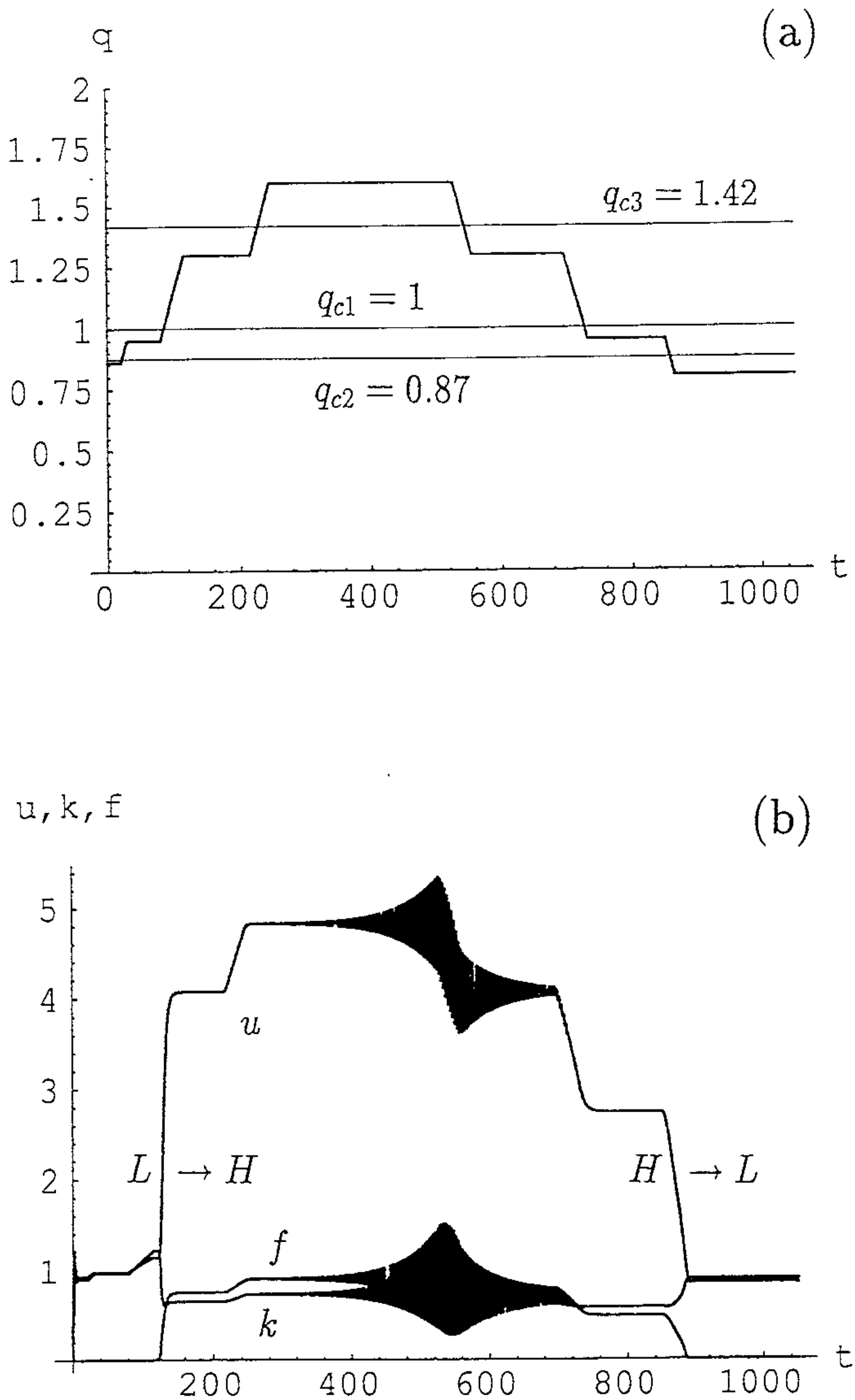

FIG.2. Numerical solutions for Case I where the energy input is temporally varied. (a) The energy input parameter q as a function of time. (b) The temporal dependence of (u, k, f).

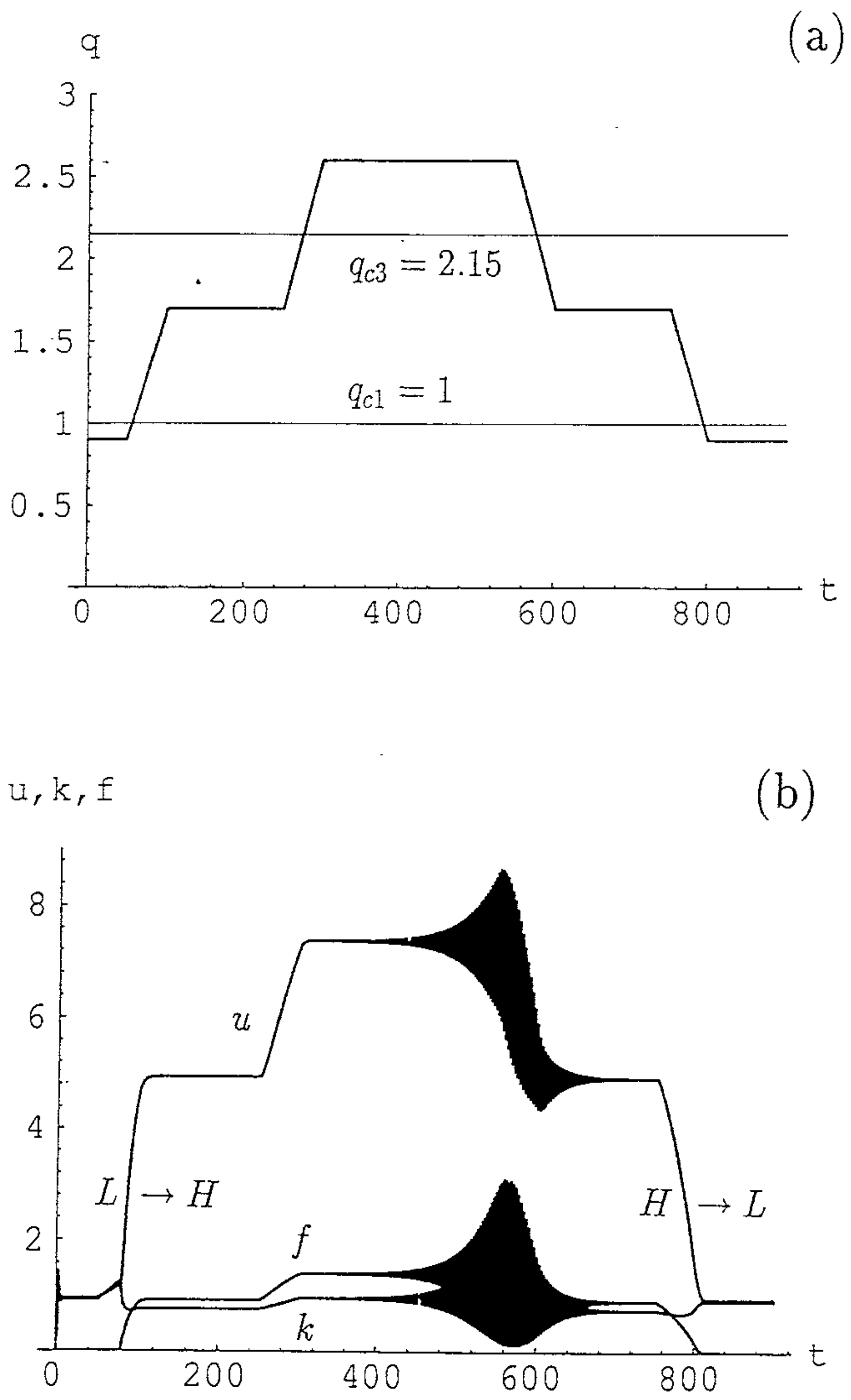

FIG.3. Numerical solutions for Case II where the energy input is temporally varied. (a) The energy input parameter q as a function of time. (b) The temporal dependence of (u, k, f).

Recent Issues of NIFS Series

NIFS-257 S. Sasaki, Y. Uesugi, S. Takamura, H. Sanuki, K. Kadota,
Temporal Behavior of the Electron Density Profile During Limiter Biasing in the HYBTOK-II Tokamak; Nov. 1993

NIFS-258 K. Yamazaki, H. Kaneko, S. Yamaguchi, K.Y. Watanabe, Y.Taniguchi, O.Motojima, LHD Group,
Design of Central Control System for Large Helical Device (LHD); Nov. 1993

NIFS-259 S. Yamada, T. Mito, A. Nishimura, K. Takahata, S. Satoh, J. Yamamoto, H. Yamamura, K. Masuda, S. Kashihara, K. Fukusada, E. Tada,
Reduction of Hydrocarbon Impurities in 200L/H Helium Liquefier-Refrigerator System; Nov. 1993

NIFS-260 B.V.Kuteev,
Pellet Ablation in Large Helical Device; Nov. 1993

NIFS-261 K. Yamazaki,
Proposal of "MODULAR HELIOTRON': Advanced Modular Helical System Compatible with Closed Helical Divertor; Nov. 1993

NIFS-262 V.D.Pustovitov,
Some Theoretical Problems of Magnetic Diagnostics in Tokamaks and Stellarators; Dec. 1993

NIFS-263 A. Fujisawa, H. Iguchi, Y. Hamada
A Study of Non-Ideal Focus Properties of 30° Parallel Plate Energy Analyzers; Dec. 1993

NIFS-264 K. Masai,
Nonequilibria in Thermal Emission from Supernova Remnants; Dec. 1993

NIFS-265 K. Masai, K. Nomoto,
X-Ray Enhancement of SN 1987A Due to Interaction with its Ring-like Nebula; Dec. 1993

NIFS-266 J. Uramoto
A Research of Possibility for Negative Muon Production by a Low Energy Electron Beam Accompanying Ion Beam; Dec. 1993

NIFS-267 H. Iguchi, K. Ida, H. Yamada, K. Itoh, S.-I. Itoh, K. Matsuoka, S. Okamura, H. Sanuki, I. Yamada, H. Takenaga, K. Uchino, K. Muraoka,
The Effect of Magnetic Field Configuration on Particle Pinch Velocity in Compact Helical System (CHS); Jan. 1994

NIFS-268 T. Shikama, C. Namba, M. Kosuda, Y. Maeda,
Development of High Time-Resolution Laser Flash Equipment for Thermal Diffusivity Measurements Usting Miniature-Size Specimens; Jan. 1994

NIFS-269 T. Hayashi, T. Sato, P. Merkel, J. Nührenberg, U. Schwenn,
Formation and 'Self-Healing' of Magnetic Islands in Finite-β Helias Equilibria; Jan. 1994

NIFS-270 S. Murakami, M. Okamoto, N. Nakajima, T. Mutoh,
Efficiencies of the ICRF Minority Heating in the CHS and LHD Plasmas; Jan. 1994

NIFS-271 Y. Nejoh, H. Sanuki,
Large Amplitude Langmuir and Ion-Acoustic Waves in a Relativistic Two-Fluid Plasma; Feb. 1994

NIFS-272 A. Fujisawa, H. Iguchi, A. Taniike, M. Sasao, Y. Hamada,
A 6MeV Heavy Ion Beam Probe for the Large Helical Device; Feb. 1994

NIFS-273 Y. Hamada, A. Nishizawa, Y. Kawasumi, K. Narihara, K. Sato, T. Seki, K. Toi, H. Iguchi, A. Fujisawa, K. Adachi, A. Ejiri, S. Hidekuma, S. Hirokura, K. Ida, J. Koong, K. Kawahata, M. Kojima, R. Kumazawa, H. Kuramoto, R. Liang, H. Sakakita, M. Sasao, K. N. Sato, T. Tsuzuki, J. Xu, I. Yamada, T. Watari, I. Negi,
Measurement of Profiles of the Space Potential in JIPP T-IIU Tokamak Plasmas by Slow Poloidal and Fast Toroidal Sweeps of a Heavy Ion Beam; Feb. 1994

NIFS-274 M. Tanaka,
A Mechanism of Collisionless Magnetic Reconnection; Mar. 1994

NIFS-275 A. Fukuyama, K. Itoh, S.-I. Itoh, M. Yagi and M. Azumi,
Isotope Effect on Confinement in DT Plasmas; Mar. 1994

NIFS-276 R.V. Reddy, K. Watanabe, T. Sato and T.H. Watanabe,
Impulsive Alfven Coupling between the Magnetosphere and Ionosphere; Apr.1994

NIFS-277 J. Uramoto,
A Possibility of π^- Meson Production by a Low Energy Electron Bunch and Positive Ion Bunch; Apr. 1994

NIFS-278 K. Itoh, S.-I. Itoh, A. Fukuyama, M. Yagi and M. Azumi,
Self-sustained Turbulence and L-mode Confinement in Toroidal Plasmas II; Apr. 1994

NIFS-279 K. Yamazaki and K.Y.Watanabe,
New Modular Heliotron System Compatible with Closed Helical Divertor and Good Plasma Confinement; Apr. 1994

NIFS-280 S. Okamura, K. Matsuoka, K. Nishimura, K. Tsumori, R. Akiyama, S. Sakakibara, H. Yamada, S. Morita, T. Morisaki,. N. Nakajima, K. Tanaka, J. Xu, K. Ida, H. Iguchi, A. Lazaros, T. Ozaki, H. Arimoto, A. Ejiri, M. Fujiwara, H. Idei. O. Kaneko, K. Kawahata, T. Kawamoto, A. Komori, S. Kubo, O. Motojima, V.D. Pustovitov, C. Takahashi, K. Toi and I. Yamada,
High-Beta Discharges with Neutral Beam Injection in CHS; Apr. 1994

NIFS-281 K. Kamada, H. Kinoshita and H. Takahashi,
Anomalous Heat Evolution of Deuteron Implanted Al on Electron Bombardment ; May 1994

NIFS-282 H. Takamaru, T. Sato, K. Watanabe and R. Horiuchi,
Super Ion Acoustic Double Layer; May 1994

NIFS-283 O.Mitarai and S. Sudo
Ignition Characteristics in D-T Helical Reactors; June 1994

NIFS-284 R. Horiuchi and T. Sato,
Particle Simulation Study of Driven Magnetic Reconnection in a Collisionless Plasma; June 1994

NIFS-285 K.Y. Watanabe, N. Nakajima, M. Okamoto, K. Yamazaki, Y. Nakamura, M. Wakatani,
Effect of Collisionality and Radial Electric Field on Bootstrap Current in LHD (Large Helical Device); June 1994

NIFS-286 H. Sanuki, K. Itoh, J. Todoroki, K. Ida, H. Idei, H. Iguchi and H. Yamada,
Theoretical and Experimental Studies on Electric Field and Confinement in Helical Systems; June 1994

NIFS-287 K. Itoh and S-I. Itoh,
Influence of the Wall Material on the H-mode Performance; June 1994

NIFS-288 K. Itoh, A. Fukuyama, S.-I. Itoh, M. Yagi and M. Azumi
Self-Sustained Magnetic Braiding in Toroidal Plasmas: July 1994

NIFS-289 Y. Nejoh,
Relativistic Effects on Large Amplitude Nonlinear Langmuir Waves in a Two-Fluid Plasma; July 1994

NIFS-290 N. Ohyabu, A. Komori, K. Akaishi, N. Inoue, Y. Kubota, A.I. Livshit, N. Noda, A. Sagara, H. Suzuki, T. Watanabe, O. Motojima, M. Fujiwara, A. Iiyoshi, *Innovative Divertor Concepts for LHD*; July 1994

NIFS-291 H. Idei, K. Ida, H. Sanuki, S. Kubo, H. Yamada, H. Iguchi, S. Morita, S. Okamura, R. Akiyama, H. Arimoto, K. Matsuoka, K. Nishimura, K. Ohkubo, C. Takahashi, Y. Takita, K. Toi, K. Tsumori and I. Yamada, *Formation of Positive Radial Electric Field by Electron Cyclotron Heating in Compact Helical System*; July 1994

NIFS-292 N. Noda, A. Sagara, H. Yamada, Y. Kubota, N. Inoue, K. Akaishi, O. Motojima, K. Iwamoto, M. Hashiba, I. Fujita, T. Hino, T. Yamashina, K. Okazaki, J. Rice, M. Yamage, H. Toyoda and H. Sugai, *Boronization Study for Application to Large Helical Device*; July 1994

NIFS-293 Y. Ueda, T. Tanabe, V. Philipps, L. Könen, A. Pospieszczyk, U. Samm, B. Schweer, B. Unterberg, M. Wada, N. Hawkes and N. Noda, *Effects of Impurities Released from High Z Test Limiter on Plasma Performance in TEXTOR*; July. 1994

NIFS-294 K. Akaishi, Y. Kubota, K. Ezaki and O. Motojima, *Experimental Study on Scaling Law of Outgassing Rate with A Pumping Parameter*, Aug. 1994

NIFS-295 S. Bazdenkov, T. Sato, R. Horiuchi, K. Watanabe *Magnetic Mirror Effect as a Trigger of Collisionless Magnetic Reconnection*, Aug. 1994

NIFS-296 K. Itoh, M. Yagi, S.-I. Itoh, A. Fukuyama, H. Sanuki, M. Azumi *Anomalous Transport Theory for Toroidal Helical Plasmas*, Aug. 1994

NIFS-297 J. Yamamoto, O. Motojima, T. Mito, K. Takahata, N. Yanagi, S. Yamada, H. Chikaraishi, S. Imagawa, A. Iwamoto, H. Kaneko, A. Nishimura, S. Satoh, T. Satow, H. Tamura, S. Yamaguchi, K. Yamazaki, M. Fujiwara, A. Iiyoshi and LHD group, *New Evaluation Method of Superconductor Characteristics for Realizing the Large Helical Device;* Aug. 1994

NIFS-298 A. Komori, N. Ohyabu, T. Watanabe, H. Suzuki, A. Sagara, N. Noda, K. Akaishi, N. Inoue, Y. Kubota, O Motojima, M. Fujiwara and A. Iiyoshi, *Local Island Divertor Concept for LHD*; Aug. 1994

NIFS-299 K. Toi, T. Morisaki, S. Sakakibara, A. Ejiri, H. Yamada, S. Morita, K. Tanaka, N. Nakjima, S. Okamura, H. Iguchi, K. Ida, K. Tsumori, S. Ohdachi, K. Nishimura, K. Matsuoka, J. Xu, I. Yamada, T. Minami, K. Narihara, R. Akiyama, A. Ando, H. Arimoto, A. Fujisawa, M. Fujiwara, H. Idei, O. Kaneko, K. Kawahata, A. Komori, S. Kubo, R. Kumazawa, T. Ozaki, A. Sagara, C. Takahashi, Y. Takita and T. Watari *Impact of Rotational-Transform Profile Control on Plasma Confinement and Stability in CHS*; Aug. 1994